Influence of the ⟨111⟩ twinning on the formation of diamond cubic/diamond hexagonal heterostructures in Cu-catalyzed Si nanowires

Jordi Arbiol,[1,2,a)] Anna Fontcuberta i Morral,[3,4] Sònia Estradé,[2] Francesca Peiró,[2] Billel Kalache,[3] Pere Roca i Cabarrocas,[3] and Joan Ramon Morante[2]

[1]*GAEN-CeMARC, Group of Advanced Electron Nanoscopy - Centre de Microscòpia d'Alta Resolució de Catalunya, Universitat de Barcelona, Lluís Solé i Sabaris 1-3, E-08028 Barcelona, Catalonia, Spain*
[2]*EME/XaRMAE/IN²UB, Departament d'Electrònica, Universitat de Barcelona, E-08028 Barcelona, Catalonia, Spain*
[3]*Laboratoire de Physique des Interfaces et Couches Minces, Ecole Polytechnique, 91128 Palaiseau Cedex, France*
[4]*Walter Schottky Institute, Technical University of Munich, Am Coulombwall 3, D-85748 Garching, Germany*

The occurrence of heterostructures of cubic silicon/hexagonal silicon as disks defined along the nanowire ⟨111⟩ growth direction is reviewed in detail for Si nanowires obtained using Cu as catalyst. Detailed measurements on the structural properties of both semiconductor phases and their interface are presented. We observe that during growth, lamellar twinning on the cubic phase along the ⟨111⟩ direction is generated. Consecutive presence of twins along the ⟨111⟩ growth direction was found to be correlated with the origin of the local formation of the hexagonal Si segments along the nanowires, which define quantum wells of hexagonal Si diamond. Finally, we evaluate and comment on the consequences of the twins and wurtzite in the final electronic properties of the wires with the help of the predicted energy band diagram. © *2008 American Institute of Physics.*
[DOI: 10.1063/1.2976338]

I. INTRODUCTION

One-dimensional systems such as quantum wires, nanowires (NWs), and nanotubes have attracted considerable attention due to their potential application in electronic, optoelectronic, sensor, and energy conversion devices, for which electrical transport as well as phonon transport play a significant role in determining their properties.[1–9] In contrast with the number of theoretical studies on transport phenomena in nanostructures, experimental investigations on the correspondence between transport mechanisms and their structural properties at the nanoscale have been scarcely reported. A detailed knowledge of the structure becomes increasingly important when solids are reduced to the nanometer range.[10] Then, transport phenomena can be significantly altered due to various effects, namely, (i) increased surface, interface, and defect scatterings, (ii) changes in phonon dispersion relation and energy bands, (iii) quantization due to the electron or/and phonon confinement, and (iv) formation of minibands.[11–15]

Among all the existing nanostructures, silicon NWs hold the promise of enabling modern electronic optoelectronic devices, as well as enabling future complementary metal oxide semiconductor (CMOS) technology nodes. Theoretical and experimental studies show that as the dimension of crystalline Si domains is reduced to a few nanometers, many of the optical and electronic transport properties are modified due to the confinement.[16–18] Likewise, molecular dynamics simulations have also shown that, for these small domains, the thermal conductivities could be even two orders of magnitude smaller than that of bulk silicon.[19] Nevertheless, in spite of the importance to understand the underlying transport physics in silicon NWs and their application in nanodevices, to the best of our knowledge, very little attention has been paid on the effect of structural peculiarities at the nanoscale of Si NWs on the measured properties. Such study would have important implications in the design and performances of modern microelectronic devices with sub-100-nm features as well as for recently proposed NW-based thermoelectric devices.[20–22]

One of the most common method for the synthesis of NWs is the vapor-liquid-solid (VLS) method, in which a metal seed catalyst is required[23] to nucleate the growth of NWs. Different metals have been proposed, and it has been found that silicon crystallization is strongly influenced by which metal is used. Al, In, and Au have been claimed to form eutectics with Si, whereas Pd and Ni are accepted to form various silicides with Si which enhance the incorporated Si atoms in a crystallized structure.[24,25] Many efforts have been centered to find other appropriate metal catalysts compatible with device processing.[26] Among the different candidates, copper has been reported to interact in a different way with silicon atoms than those other metal catalysts forming eutectics (gold) and silicides (nickel). During the process of metal-induced recrystallization of amorphous silicon, the metal atoms appear to enhance the crystallization of amorphous silicon. It is believed that the metal atoms are repelled by the crystalline silicon (c-Si) whereas Si atoms from the amorphous silicon (a-Si) migrate into the c-Si side, resulting

in crystallization. When using Cu as a metal, higher crystallization rates are obtained, in comparison to other commonly used metals, such as Ni and Au.[27] Within this logic, Kalache and co-workers[28,29] recently synthesized silicon NWs by using Cu as catalyst. In addition, the use of Cu instead of Au when synthesizing Si NWs avoids the cross-contamination issues and thus the incompatibility with CMOS technology, letting the NWs enter the field of low-dimensional semiconductor structures, future CMOS technology, and nano-optoelectronic devices.[28] In a previous paper, we performed a preliminary analysis of the Si NWs grown by using Cu as catalyst;[29] we studied them at different temperatures from 500 to 650 °C. For higher temperatures (600 and 650 °C) we found the formation of grain boundaries along the [111] growth direction. Deeper analysis and modeling were needed for a complete understanding.

In this paper we review in detail the structural characteristics of silicon NWs synthesized with Cu as a catalyst and discuss the relation with the growth mechanism. Initially, high resolution transmission electron microscopy measurements that indicate the presence of lamellar twinning along the growth direction are presented. The experimental results are analyzed showing that the multiplicity of $\langle 111 \rangle$ twinning can generate local changes in the stacking sequence of the diamond structure, leading to a Si diamond cubic/hexagonal heterostructure. Second, we present the energy band diagram and the conduction band potential profile of the resulting quantum well (QW) heterostructure to illustrate how its presence may alter the NW electrical and thermal transport properties.

Finally, a detailed study of the structural properties between both semiconductor phases and NW morphology are reported and plausible growth models are discussed.

II. EXPERIMENTAL DETAILS

Silicon NWs were synthesized by catalytic chemical vapor deposition (CVD). Thermally oxidized silicon wafers (oxide thickness of 1 μm) covered with an equivalent 3 nm Cu layer were used as substrates. Once diced in $\sim 2 \times 2$ cm^2, the sample pieces were heated under vacuum and under flow of 100 SCCM (SCCM denotes cubic centimeter per minute at STP) of H$_2$ 5 min prior to deposition in order to get a uniform temperature through the substrate. For the silicon NW synthesis, 2.5% silane was added to the hydrogen flow. At temperatures below the pyrolysis, silane is known to catalytically decompose only at the surface of the metal.[30] The CVD runs were realized at temperatures between 600 and 650 °C for a duration of 15 min, giving rise to NWs of several microns in length. More details on NW synthesis can be found elsewhere.[28] The morphology and structure at the nanoscale were characterized with high-resolution transmission electron microscopy (HRTEM) and scanning transmission electron microscopy (STEM) in bright-field (BF) (BFSTEM) and high angular annular dark field (HAADF) (HAADF-STEM) modes. The three-dimensional (3D) atomic models presented were designed by using the RHODIUS software package.[31]
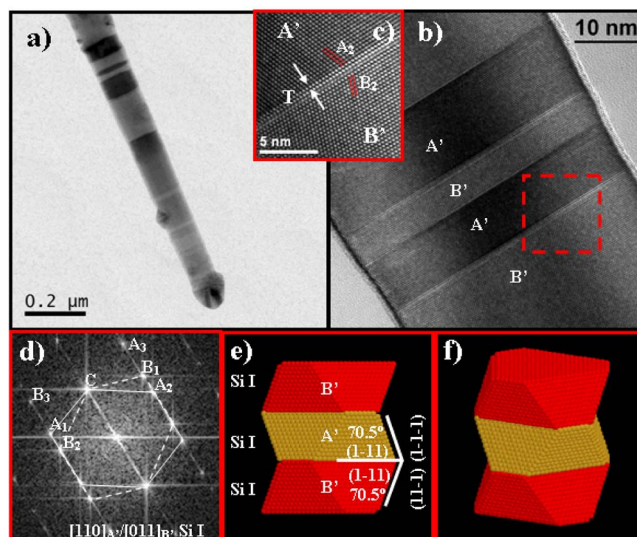

FIG. 1. (Color online) (a) BFSTEM general view of a Si NW with lamellar $\langle 111 \rangle$ twinning. (b) HRTEM micrograph of the twin segments. (c) Magnified detail of the squared region in (b). (d) Indexed power spectrum obtained in (c). (e) 3D atomic model proposed following theoretical models on III-V semiconductor NWs (model A) (a 3D animated movie of the present model can be found in http://nun97.el.ub.es/~arbiol/Work001.html). (f) Same model in perspective.

III. RESULTS AND DISCUSSION

We have separated this section into three different parts with the purpose of emphasizing the key points: NW morphology and faceting, $\langle 111 \rangle$ twinning and cubic/hexagonal heterostructure, and Si I/Si IV energy band properties.

A. NW morphology and faceting

Following previous morphological models of GaP NW faceting,[32] we have built a model for our Si NWs, as shown in Figs. 1(e) and 1(f). The twin segments have an octahedral shape and are terminated by [111] facets, resulting in a "nanofaceted" morphology of the NWs. However, NW faceting does not always follow this casuistic, and modeling can be more difficult and require a more detailed analysis.[33,34] A more complex analysis of the NW faceting geometry is shown in Fig. 2. In Fig. 2(a) a planar view projection of a Si NW perpendicular to the growth axis can be seen. The wire has a perfect hexagonal cross section, in good agreement with the $\langle 112 \rangle$ lateral faceting and $[1-11]$ growth direction (confirmed by electron diffraction patterns, not shown here). In Fig. 2(b) a HAADF-STEM profile along a domain of a NW is presented (course indicated by a dashed line). A selected area electron diffraction spectrum was taken on the circled area indicating an orientation along the $[110]_{A'} \| [011]_{B'}$ zone axis, coinciding perfectly with the one shown and indexed in Fig. 1(d). The intensity profile obtained along the NW section [Fig. 1(d)] which is proportional to the wire thickness in every point (HAADF-STEM image with no changes in Z) indicates again a clear hexagonal section morphology of the wire. Attending to these last results, a new 3D atomic model is proposed for our Si NW morphology [Figs. 2(e)–2(g)].
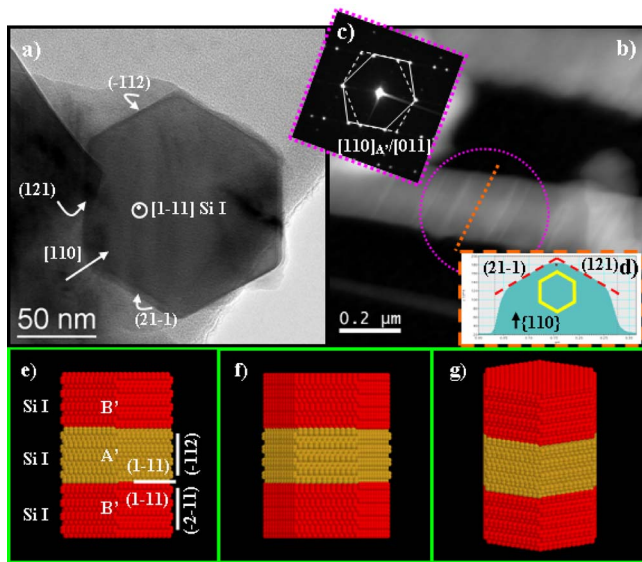
FIG. 2. (Color online) (a) Plan view TEM micrograph of a Si NW. (b) HAADF-STEM image of a twinned NW. (c) Selected area electron diffraction pattern obtained in the circled area in (b). (d) Intensity profile obtained from the dashed line in (b). (e) Experimental 3D model obtained after indexation and morphology analysis (model b) (a 3D animated movie of the present model can be found in http://nun97.el.ub.es/~arbiol/Work001.html). (f) Same model rotated 30° around the growth axis (⟨112⟩ projection). (g) Same model in perspective.

Finally, attending to the structural properties of the cubic hexagonal heterostructure, taking into account the projection faceting angles observed [Fig. 3(a)], and in comparison with previous morphological models observed in III-V (Refs. 32
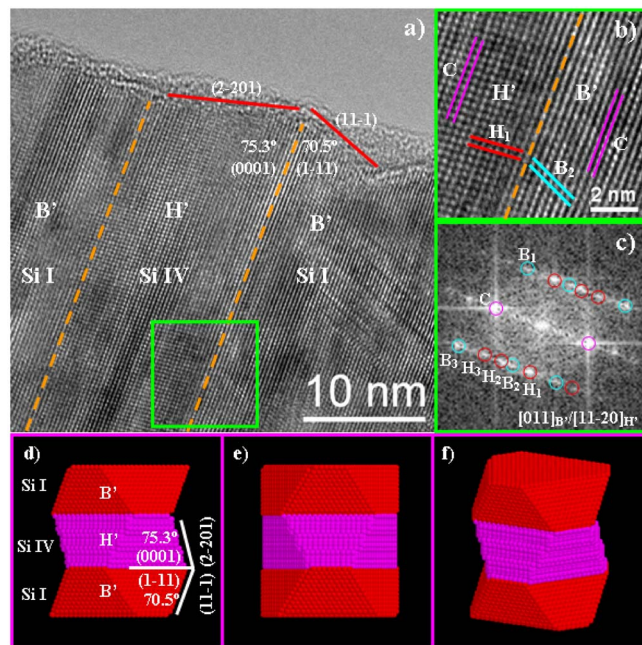

FIG. 3. (Color online) (a) HRTEM micrograph of the Si I/Si IV/Si I heterostructure. (b) Magnified detail of the squared region in (a). (c) Indexed power spectrum obtained in (b). (a)–(c) were published in Ref. 29. (d) Experimental 3D model obtained after indexation and morphology analysis of the heterostructure (model c) (a 3D animated movie of the present model can be found in http://nun97.el.ub.es/~arbiol/Work001.html). (e) Same model rotated 30° around the growth axis (⟨112⟩$_{B'}$ projection). (f) Same model in perspective.

TABLE I. Indexation of the spots corresponding to the A′ segment in Fig. 1(d).

A′ spot	d (nm), experimental	Versus spot C (°), experimental	Indexation proposed	d (nm), theoretical	Versus spot C (°), theoretical
C	0.315	⋯	(1−11)	0.313	⋯
A_1	0.269	55	(002)	0.271	54.7
A_2	0.311	71	(1−1−1)	0.313	70.5
A_3	0.191	36	(2−20)	0.192	35.3
Zone axis: [110] Si I					

and 36) and sawtooth faceted Si NWs,[35] we propose a 3D atomic model of the heterostructure morphology [Figs. 3(d)–3(f)]. Si I segments (B′) grow along the [1−11] axis, while Si IV segments grow along the [0001] axis. Both segments have octahedral morphology, with ⟨111⟩ and ⟨2−201⟩ lateral facets for Si I and Si IV volumes, respectively. The model reported has particular angular characteristics between the growth planes and the lateral facets: angle between (1−11) and (11−1) for segment B′ and angle between (0001) and (2−201) for the H′ segment. The lateral faceting angle between the projected facets and the growth planes are in good agreement with the experimental calculated faceting angle observed in ⟨011⟩$_{B'}$ and ⟨11−20⟩$_{H'}$ projections [Fig. 3(a)], which corresponds to 70.5° and 75.3°, respectively. In this case the original ⟨111⟩ faceting angles of the octahedral B′ segment are still visible.

B. ⟨111⟩ twinning and cubic/hexagonal heterostructure

In Fig. 1(a) we show a BFSTEM micrograph of a Si NW presenting lamellar twinning features along the ⟨111⟩ growth axis. This measurement is representative of more than 90% of the analyzed NWs (around 50). Only a few NWs have been found to grow along the ⟨112⟩ growth axis. As shown in Figs. 1(a) and 1(b), the lamellae are recognized by bright and dark stripes and only by HRTEM is it possible to determine the structural nature of the domains [Figs. 1(b) and 1(c)]. HRTEM has been realized in order to analyze the structural properties of the dark and bright domains. As observed in the power spectrum (fast Fourier transform) shown in Fig. 1(d), both domains (labeled as A′ and B′) keep the same growth axis, being [1−11] (spot labeled as C, common for both domains). For further clarification, the indexation results of the domains are presented in Tables I and II. We find that the twin boundary divides both segments with a 60° rotation of

TABLE II. Indexation of the spots corresponding to the B′ segment in Fig. 1(d).

B′ spot	d (nm), experimental	Versus spot C (°), experimental	Indexation proposed	d (nm), theoretical	Versus spot C (°), theoretical
C	0.315	⋯	(1−11)	0.313	⋯
B_1	0.269	55	(200)	0.271	54.7
B_2	0.311	70	(−1−11)	0.313	70.5
B_3	0.193	36	(0−22)	0.192	35.3
Zone axis: [011] Si I					

the diamond cubic structure with respect to the $[1-11]$ growth axis. This particular reorientation of the crystal does not involve any bond breaking and results in a planar reflection of the stacking order of the {111} planes. A′ and B′ twin domains alternate without periodicity along the growth axis with the following epitaxial relationship: $(1-11) \times [110]_{\text{Si I}} \| (1-11)[011]_{\text{Si I}}$, meaning that the growth plane $(1-11)$ observed along the $[110]$ zone axis in the A′ segment is parallel to the $(1-11)$ growth plane observed in the $[011]$ zone axis in the B′ segment. This phenomenon, characterized by a change in the regular *abcabc* stacking of close-packed layers to *abc/bac*, with "/" denoting the twin plane, has been referred to as lamellar twinning.[36] The dark and bright contrast regions observed in our NWs are the result of the image being taken with the electron beam oriented slightly off the $[110]$ crystallographic axis.[36] Nonlamellar twins in Si NWs have already been observed but only in NWs grown on the $\langle 112 \rangle$ zone axis. In this case, the twins were found in {111} facets, following the entire length of the NWs.[37–39] In a recent paper Yao and Fan[40] synthesized Si NWs by using Cu as catalyst at the low temperature of 500 °C. In their case, Si NWs showed the presence of {111} stacking faults (SFs) and microtwins; however, the main part of {111} twins and SFs were found crossing the NWs diagonally and only a few SFs were found on the {111} growth planes, thus not forming twin segments on the growth axis. Their diffraction patterns showed only evidence of a simple cubic structure with no rotation present. Nevertheless, in the present work, lamellar twinning along the growth axis (with {111} twin segments parallel to the {111} growing planes) has been observed and described in detail in silicon wires grown along the $\langle 111 \rangle$ direction. Lamellar twins in NWs (e.g., in III-V group materials) have already centered many efforts due to their consequences in transport mechanisms. A recent study performed by Davidson *et al.*[36] postulated that $\langle 111 \rangle$ twins along the $\langle 111 \rangle$ growth direction were not expected to appear in Au-seeded Si NWs grown by the VLS mechanism. Twinning during growth is only possible when the change in the angle of the sidewalls of the NW during twinning does not induce the dewetting of the metal catalyst, leading to the slide off the tip of the wire. This depends of course on the metal and the NW material. With this assumption, it was predicted that lamella twinning of Si NWs could not occur when Au is used as a catalyst; thus the growth followed the VLS mechanism. By just changing the metal catalyst or the material (III-V semiconductors, for example), twinning should be possible. In agreement with the theoretical predictions of Davidson *et al.*,[36] twinning is indeed a widely observed effect experimentally in group III-V semiconductor NWs.[32,34,36,41–43] Johansson *et al.*[32] proposed another growth model for lamellar twinning in GaP NWs, in which they concluded that twin nucleation is a consequence of fluctuations in mass transport as well as thermal fluctuations. We believe that there is an added reason for the different structure of NWs synthesized with Cu as a catalyst. We have observed that the growth follows a vapor-solid-solid (VSS) mechanism instead of the VLS typically observed with Au.[28] Precipitation from a solid alloy in comparison to the precipitation from a liquid melt may affect the final structure in different aspects: (i) The Si atoms should be less "mobile," giving rise to an easier defect formation; however, a low mobility should also manifest itself in polycenter nucleation and eventually in rough growth, which has not been observed and which, in fact, would only be an issue if the nucleation rate was higher than the time it takes to complete the full layer, i.e., the flow in "step-flow" growth. (ii) With the VSS synthesis, a pseudoepitaxial relation can exist between the solid alloy and the precipitated atoms, possibly enhancing the effect of the successive layer-by-layer atomic arrangement during growth. In any case both points are speculative and should be further studied. Additionally, we would like to point out that the NWs have similar structural characteristics than those found in Cu-induced recrystallized amorphous silicon.[44] It has been indeed shown that, when using Cu for the recrystallization of amorphous silicon, Si crystallites (needles) embedded in an amorphous Si layer are formed. These crystallites also seem to grow along the $\langle 111 \rangle$ axis and present multiple twinning on the growth direction.

Now we would like to go one step further in the discussion of the lamellar twinning and evaluate the physical consequences. It is widely known that in group III-V semiconductors, a sequence of $\langle 111 \rangle$ SFs may result in a local change in the stacking sequence of atomic planes in the NWs.[45] Thus, in the case of III-V compounds, if the NW exhibits the diamond cubic zinc-blende structure, the formation of 60° rotational twin along the $\langle 111 \rangle$ growth axis results in a local change in the stacking of the {111}-type close-packed planes, resulting in the formation of a local region of the hexagonal wurtzite structure.[45–48] As a consequence, the formation of successive faulty stacking on {111} planes of the zinc-blende structure could result in a complete transformation to the hexagonal wurtzite structure (Fig. 4). In the present case, the *abcabc* arrangement of close-packed atomic layers in the $\langle 111 \rangle$ planes of the diamond cubic structure (Si I polytype in the case of Si) [Fig. 4(a)] can change to the *a″b″a″b″a″* arrangement of the $\langle 0001 \rangle$ planes of the diamond hexagonal or wurtzite structure (Si IV polytype in the case of Si), see Fig. 4 and also Refs. 49–52. At this point it is important to note that Si NWs synthesized until now by many research groups have been often found to crystallize in the conventional diamond cubic Si structure (Si I polytype).[53–55] Nevertheless, it is known that Si can crystallize in some other structural phases, though these structures are generally found under extreme growth conditions (high pressure and/or high temperature).[56] Several forms of silicon have been obtained when applying high pressures (up to 50 GPa). Nevertheless, just four of them have been found to remain stable or metastable at ambient: Si I, *a*-Si, Si III, and Si IV, the first two being classical device materials.[57]

Hiruma *et al.*[58] attributed the density of growth twins in GaAs NWs to the competing stabilities of the zinc-blende and wurtzite polytypic forms of this compound. Attending to these considerations, the mere existence of $\langle 111 \rangle$ twins in our Si NWs should lead to the formation of local diamond hexagonal regions such as it has been found, see Fig. 3. Figure 3(a) shows a BFTEM general view of a Si NW with lamellar twinning along the growth axis. If we have a closer look at the wire [Fig. 5(b)] we can find regions where the periodicity
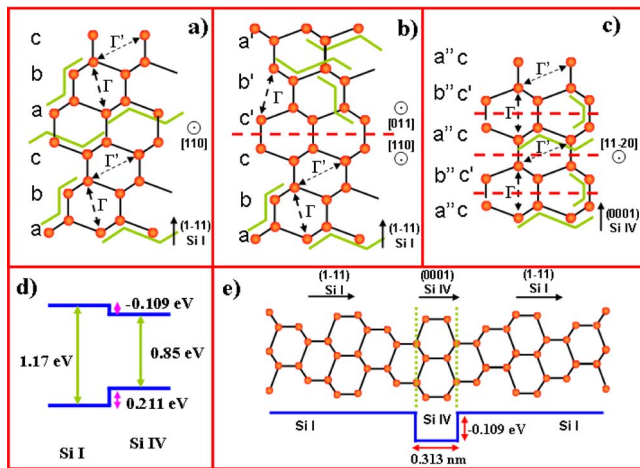
FIG. 4. (Color online) (a) Regular *abcabc* stacking of close-packed layers in diamond cubic Si (Si I polytype). (b) Cubic close-packed stacking with a twin *abc/c'b'a'*, with "/" and dashed line in the figure denoting the twin. *c'*, *b'*, and *a'* correspond to the *c*, *b*, and *a* planes after the twin 60° rotation along the growth axis. (c) *a"b"a"b"a"* or equally *c/c'/c/c'/c* arrangement of the ⟨0001⟩ planes on the diamond hexagonal or wurtzite structure (Si IV polytype), dashed lines denoting the inverse domains due to twins. (d) Schematics of the energy position of the minimum and maximum of the conduction and valence bands, respectively, of the Si I / Si IV heterostructure according to Refs. 59 and 60. It should be noted that the positions correspond to different valleys in the reciprocal space. (e) Similar band alignment diagram for a quantum heterostructure, formed by a single Si IV unit (0.313 nm) (marked between dashed lines), generated by a 60° rotational twin. As shown in the paper, the thickness of the generated QW can change depending on the number (n) of Si IV units ($n \times 0.313$ nm).

of twins is higher. A detailed analysis of one of these regions [Fig. 5(c)] shows a narrow segment composed of four consecutive twins, leading to an *a"b"a"b"a"* arrangement typical of the diamond hexagonal structure. Accurate analysis and indexation of the power spectrum on the squared area
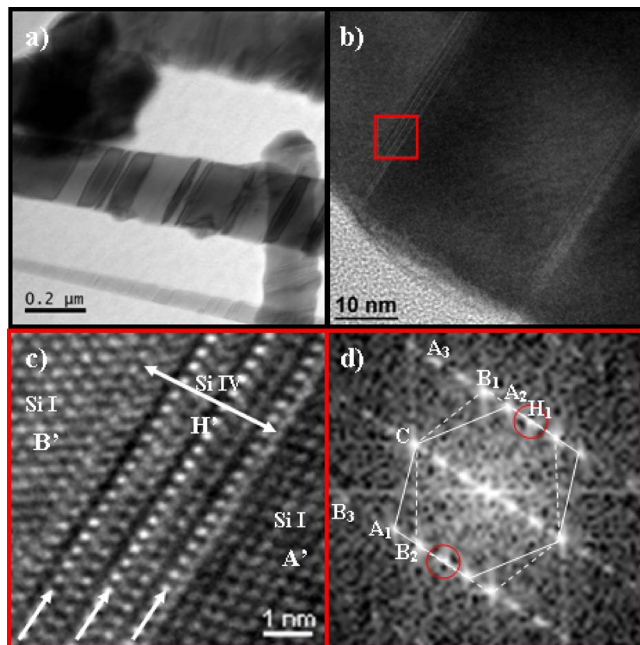

FIG. 5. (Color online) (a) TEM general view of a synthesized NW. (b) HRTEM detail of the twin segments. (c) Magnified detail of the squared region in (b) showing a multitwinned segment leading to a diamond hexagonal local region. (d) Indexed power spectrum obtained in (c).

TABLE III. Indexation of the spots corresponding to the H′ segment in Fig. 4(c).

H′ spot	d (nm), experimental	Versus spot C (°), experimental	Indexation proposed	d (nm), theoretical	Versus spot C (°), theoretical
C	0.313	⋯	(0002)	0.313	⋯
H_1	0.327	86	(1−100)	0.329	90
H_2	0.294	65	(1−101)	0.291	62
H_3	0.242	48	(1−102)	0.227	44
			Zone axis: [11−20] Si IV		

have been performed [Fig. 5(d)]. The A_x and B_x spots corresponds to the A′ and B′ regions just below and above the Si IV region (H′) and can be indexed as those found in Fig. 1(d) (Tables I and II). However, a new reflection appears on the pattern (circled and labeled as H_1), which corresponds to the diamond hexagonal (1−100) plane (with an atomic interplanar distance of 0.329 nm).

In a previous work,[29] we showed that Si IV could be found forming extended regions up to a few nanometers. In Fig. 3, we show an example of a thick QW (10 nm) [similar figures to Figs. 3(a)–3(c) were published in our previous work dealing on Si NW synthesis by using Cu as catalyst[29]). A magnified detail is shown in Fig. 3(b), which has been analyzed and indexed by using its power spectrum [Fig. 3(c) and Tables III and IV]. Here it should be noted that the cell parameters found experimentally for the diamond hexagonal segment are slightly distorted with respect to the theoretical one (see Table III), which makes us think that the diamond hexagonal segment is stressed. An epitaxial relationship between both structures has been obtained: (1−11) ×[110]$_{\text{Si I}}$‖(0001)[11−20]$_{\text{Si IV}}$, the (1−11)$_{\text{Si I}}$ and (0001)$_{\text{Si IV}}$ being the atomic growth planes for diamond cubic and diamond hexagonal structural phases, respectively, which are the only ones from silicon that present semiconductor characteristics. Interestingly enough is that the epitaxial relationship found on this heterostructure (Si I/Si IV) perfectly coincides with the reported zinc-blende/wurtzite heterostructure in the case of GaAs NWs.[47] Furthermore, this is the same epitaxial relationship observed between the Si I and Si IV regions observed by Pirouz *et al.*,[50–52] in bulk Si martensitic deformations induced under high pressure conditions.

C. Si I/Si IV energy band properties

From the examples shown above in Figs. 1, 3, and 5, it is possible to conclude that the diamond hexagonal structure

TABLE IV. Indexation of the spots corresponding to the B′ segment in Fig. 4(c).

B′ spot	d (nm), experimental	Versus spot C (°), experimental	Indexation proposed	d (nm), theoretical	Versus spot C (°), theoretical
C	0.313	⋯	(1−11)	0.313	⋯
B_1	0.274	56	(200)	0.271	55
B_2	0.320	71	(−1−11)	0.313	71
B_3	0.191	35	(0−22)	0.192	35
			Zone axis: [011] Si I		

can be found at different extents from a single unit or mono-layer [when the presence of a single twin is present, see model in Fig. 4(e)], up to a few nanometers. As silicon with diamond hexagonal structure (Si IV) has been reported to present a semiconductor behavior,[57] the mere presence of Si IV inclusions leads to the creation of QWs along the growth ⟨111⟩ axis with different thicknesses. QW thicknesses would depend on the multiplicity or density of twin defects on the cubic structure, with the cubic diamond silicon regions acting as QW barriers. In the following, we will present the band structure of the wurtzite/zinc-blende silicon heterostructure and deduce what the consequences would be for the optical and electronic properties of the NWs.

Si IV polytype is reported to present a smaller band gap, ∼0.85 eV, than the cubic diamond silicon, 1.17 eV.[59] The minimum energy for the conduction band in Si I is placed in the X symmetry direction,[59] thus denoting an indirect band gap. In the case of Si IV with a diamond hexagonal structure, the conduction band minimum is found at the M direction, meaning that it also exhibits an indirect band gap. The fact that the two structures have a minimum in the conduction band in different symmetry points complicates the analysis of the heterostructure. In order to understand the possibility of carrier confinement in this type of heterostructures, we have aligned the minimum and maximum of the conduction and valence bands, respectively, in a plot [Fig. 4(d)]. The energy difference between the lowest conduction band state at M for Si IV and at X for Si I was calculated to be −0.109 eV,[60] while for the valence band, it is 0.211 eV. First of all, this means that the heterostructure has a type I alignment. In the case of formation of quantum heterostructures such as QWs, this means that it is possible to have confinement of electrons and holes if the QW has a Si IV structure.

From these plots, it is straightforward to deduce that the existence of Si I and Si IV phases must alter the transport, modifying electron and phonon parameters. These characteristics make coherent electron transport difficult but open new possibilities in the area of band-structure engineering (Fig. 2) for optical and thermoelectric applications. As an example, Bao *et al.*[61] showed in a recent work how the presence of multitwins and related wurtzite quantum domains in InP NWs could influence their photoluminescence properties. In their case, the excitation power dependent blueshift of the observed photoluminescence could be explained in terms of the predicted staggered band alignment of the rotationally twinned zinc-blende/wurtzite InP heterostructure and of the concomitant diagonal transitions between localized electron and hole states responsible for radiative recombination. This is not the case of Si, where the indirect band gap minimizes the radiative recombination, but the band structure of the heterostructure is similar to the one proposed above, and thus in our case affects the transport properties along NWs. However, it has been shown that a dense sequence of axial heterostructures in NWs has a very positive effect on the thermoelectric properties.[22,62,63] We believe that this may be one of the most interesting applications in the presented NWs.

IV. CONCLUSIONS

In summary, we have reviewed the formation of lamellar twinning along the ⟨111⟩ direction in Si NWs synthesized by using Cu as catalyst. The multiple presence of the ⟨111⟩ twin defects originate the local formation of the Si diamond hexagonal segments along the NWs. The presence of multidomains may affect both the electronic and thermal transport properties in the wires and related devices. The results are therefore of great technological importance. Moreover, as the diamond hexagonal silicon domain, Si polytype–IV, has an associated different band structure than diamond cubic silicon, Si polytype–I, it defines a QW along the NW transport direction. The twinning and change in the stacking process are related to the growth mechanism of silicon NWs with Cu as a catalyst and opens new understanding on a more general model for the growth that could be extrapolated to other metal catalysts. The final goal would be the control of the periodicity of faults and morphology of the wires to develop future electronic, optoelectronic, and thermoelectric nanodevices.

[1] T. Koester, F. Goldschmidtboeing, B. Hadam, J. Stein, S. Altmeyer, B. Spangenberg, H. Kurz, R. Neumann, K. M. Brunner, and G. Abstreiter, Jpn. J. Appl. Phys., Part 1 **38**, 465 (1999).

[2] S. F. Fischer, G. Apetrii, U. Kunze, D. Schuh, and G. Abstreiter, Nat. Phys. **2**, 91 (2006).

[3] H. Pettersson, J. Tragardh, A. I. Persson, L. Landin, D. Hessman, and L. Samuelson, Nano Lett. **6**, 229 (2006).

[4] S. De Franceschi, J. A. van Dam, E. P. A. M. Bakkers, L. F. Feiner, L. Gurevich, and L. P. Kouwenhoven, Appl. Phys. Lett. **83**, 344 (2003).

[5] F. Hernández-Ramírez, A. Tarancón, O. Casals, J. Arbiol, A. Romano-Rodríguez, and J. R. Morante, Sens. Actuators B **121**, 3 (2007).

[6] J. Arbiol, E. Comini, G. Faglia, G. Sberveglieri, and J. R. Morante, J. Cryst. Growth **310**, 253 (2008).

[7] J. Arbiol, A. Cirera, F. Peiró, A. Cornet, J. R. Morante, J. J. Delgado, and J. J. Calvino, Appl. Phys. Lett. **80**, 329 (2002).

[8] A. F. I. Morral, D. Spirkoska, J. Arbiol, M. Heigoldt, J. R. Morante, and G. Abstreiter, Small **4**, 899 (2008).

[9] F. Furtmayr, M. Vielemeyer, M. Stutzmann, J. Arbiol, S. Estradé, F. Peiró, J. R. Morante, and M. Eickhoff, J. Appl. Phys. **104**, 034309 (2008).

[10] J. D. Prades, J. Arbiol, A. Cirera, J. R. Morante, and A. F. I. Morral, Appl. Phys. Lett. **91**, 123107 (2007).

[11] C. W. J. Beenakker, Rev. Mod. Phys. **69**, 731 (1997).

[12] L. D. Hicks and M. S. Dresselhaus, Phys. Rev. B **47**, 16631 (1993).

[13] N. Mingo, L. Yang, D. Li, and A. Majumdar, Nano Lett. **3**, 1713 (2003).

[14] D. G. Cahill, W. K. Ford, K. E. Goodson, G. D. Mahan, A. Majumdar, H. J. Maris, R. Merlin, and S. R. Phillpot, J. Appl. Phys. **93**, 793 (2003).

[15] S. De Franceschi, R. Hanson, W. G. van der Wiel, J. M. Elzerman, J. J. Wijpkema, T. Fujisawa, S. Tarucha, and L. P. Kouwenhoven, Phys. Rev. Lett. **89**, 156801 (2002).

[16] G. D. Sanders and Y.-D. Chang, Phys. Rev. B **45**, 9202 (1992).

[17] H. A. Brus, J. Phys. Chem. **98**, 3575 (1994).

[18] M. L. Brongersma, P. G. Kik, A. Polman, K. S. Min, and H. A. Atwater, Appl. Phys. Lett. **76**, 351 (2000).

[19] A. Balandin and K. L. Wang, Phys. Rev. B **58**, 1544 (1998).

[20] C. Dames and G. Chen, J. Appl. Phys. **95**, 682 (2004).

[21] J. Keyani, A. M. Stacy, and J. Sharp, Appl. Phys. Lett. **89**, 233106 (2006).

[22] A. I. Hochbaum, R. Chen, R. Diaz Delgado, W. Liang, E. C. Garnett, M. Najarian, A. Majumdar, and P. Yang, Nature (London) **451**, 163 (2008).

[23] R. S. Wagner and W. C. Ellis, Appl. Phys. Lett. **4**, 89 (1964).

[24] M. H. Brodsky and D. Turnbull, Bull. Am. Phys. Soc. **16**, 304 (1971).

[25] G. Ottaviani, D. Sigurd, V. Marrello, J. W. Mayer, and J. O. McCaldin, J. Appl. Phys. **45**, 1730 (1974).

[26] V. A. Nebol'sin and A. A. Shchetinin, Inorg. Mater. **39**, 899 (2003).

[27] Y.-C. Her, C.-W. Chen, and C.-L. Wu, J. Appl. Phys. **99**, 113512 (2006).

[28] B. Kalache, P. R. I. Cabarrocas, and A. F. I. Morral, Jpn. J. Appl. Phys., Part 2 **45**, L190 (2006).

[29] J. Arbiol, B. Kalache, P. R. I. Cabarrocas, J. R. Morante, and A. F. I.

Morral, Nanotechnology **18**, 305606 (2007).

[30]S. Hymes, S. P. Muraka, C. Shepard, and W. A. Lanford, J. Appl. Phys. **71**, 4623 (1992).

[31]S. Bernal, F. J. Botana, J. J. Calvino, C. Lopez-Cartes, J. A. Perez-Omil, and J. M. Rodriguez-Izquierdo, Ultramicroscopy **72**, 135 (1998).

[32]J. Johansson, L. S. Karlsson, C. P. T. Svensson, T. Mårtensson, B. A. Wacaser, K. Deppert, L. Samuelson, and W. Seifert, Nat. Mater. **5**, 574 (2006).

[33]M. A. Verheijen, R. E. Algra, M. T. Borgstrom, G. Immink, E. Sourty, W. J. P. van Enckevort, E. Vlieg, and E. P. A. M. Bakkers, Nano Lett. **7**, 3051 (2007).

[34]L. S. Karlsson, K. A. Dick, J. B. Wagner, J. O. Malm, K. Deppert, L. Samuelson, and L. R. Wallenberg, Nanotechnology **18**, 485717 (2007).

[35]F. Ross, J. Tersoff, and M. Reuter, Phys. Rev. Lett. **95**, 146104 (2005).

[36]F. M. Davidson, D. C. Lee, D. D. Fanfair, and B. A. Korgel, J. Phys. Chem. C **111**, 2929 (2007).

[37]A. H. Carim, K.-K. Lew, and J. M. Redwing, Adv. Mater. (Weinheim, Ger.) **13**, 1489 (2001).

[38]T. Hanrath and B. A. Korgel, Small **1**, 717 (2005).

[39]Q. Tang, X. Liu, T. I. Kamins, G. S. Solomon, and J. S. Harris, Appl. Phys. Lett. **81**, 2451 (2002).

[40]Y. Yao and S. Fan, Mater. Lett. **61**, 177 (2007).

[41]A. Mikkelsen, N. Sköld, L. Ouattara, M. Borgström, J. N. Andersen, L. Samuelson, W. Seifert, and E. Lundgren, Nat. Mater. **3**, 519 (2004).

[42]A. Fontcuberta i Morral, C. Colombo, G. Abstreiter, J. Arbiol, and J. R. Morante, Appl. Phys. Lett. **92**, 063112 (2008).

[43]A. Fontcuberta i Morral, K. Maslov, C. Colombo, G. Abstreiter, J. Arbiol, and J. R. Morante, Appl. Phys. Lett. **92**, 149903 (2008).

[44]S. B. Lee, D.-K. Choi, and D. N. Lee, J. Appl. Phys. **98**, 114911 (2005).

[45]R. Banerjee, A. Bhattacharya, A. Genc, and B. M. Arora, Philos. Mag. Lett. **86**, 807 (2006).

[46]S.-G. Ihn, J.-I. Song, Y.-H. Kim, and J. Y. Lee, Appl. Phys. Lett. **89**, 053106 (2006).

[47]S.-G. Ihn, J.-I. Song, T.-W. Kim, D.-S. Leem, T. Lee, S.-G. Lee, E. K. Koh, and K. Song, Nano Lett. **7**, 39 (2007).

[48]J. Johansson, B. A. Wacaser, K. A. Dick, and W. Seifert, Nanotechnology **17**, S355 (2006).

[49]A. Fontcuberta i Morral, J. Arbiol, J. D. Prades, A. Cirera, and J. R. Morante, Adv. Mater. (Weinheim, Ger.) **19**, 1347 (2007).

[50]P. Pirouz, R. Chaim, U. Dahmen, and K. H. Westmacott, Acta Metall. Mater. **38**, 313 (1990).

[51]U. Dahmen, K. H. Westmacott, P. Pirouz, and R. Chaim, Acta Metall. Mater. **38**, 323 (1990).

[52]P. Pirouz, U. Dahmen, K. H. Westmacott, and R. Chaim, Acta Metall. Mater. **38**, 329 (1990).

[53]N. N. Kulkarni, J. Bae, C.-K. Shih, S. K. Stanley, S. S. Coffee, and J. G. Ekerdt, Appl. Phys. Lett. **87**, 213115 (2005).

[54]S.-M. Liu, M. Kobayashi, S. Sato, and K. Kimura, Chem. Commun. (Cambridge) **37**, 4690 (2005).

[55]L. Pan, K.-K. Lew, J. M. Redwing, and E. C. Dickey, Nano Lett. **5**, 1081 (2005).

[56]S. J. Duclos, Y. K. Vohra, and A. L. Ruoff, Phys. Rev. B **41**, 12021 (1990).

[57]J. M. Besson, E. H. Mokhtari, J. Gonzalez, and G. Weill, Phys. Rev. Lett. **59**, 473 (1987).

[58]K. Hiruma, M. Yazawa, K. Haraguchi, K. Ogawa, T. Katsuyama, M. Koguchi, and H. Kakibayashi, J. Appl. Phys. **74**, 3162 (1993).

[59]J. D. Joannopoulos and M. L. Cohen, Phys. Rev. B **7**, 2644 (1973).

[60]M. Murayama and T. Nakayama, Phys. Rev. B **49**, 4710 (1994).

[61]J. Bao, D. C. Bell, F. Capasso, J. B. Wagner, T. Mårtensson, J. Trägårdh, and L. Samuelson, Nano Lett. **8**, 836 (2008).

[62]D. G. Cahill, K. Goodson, and A. Majumdar, J. Heat Transfer **124**, 223 (2002).

[63]A. I. Boukai, Y. Bunimovich, J. Tahir-Kheli, Y. K. Yu, W. A. Goddard, and J. R. Heath, Nature (London) **451**, 168 (2008).